# Influence of microstructure and heat treatment on thermal conductivity of rheocast and liquid die cast Al-6Si-2Cu-Zn alloy

M. Payandeh, E. Sjölander, A. E. W. Jarfors & M. Wessén

Published online: 19 Feb 2016.

Submit your article to this journal ⬈

View related articles ⬈

# Influence of microstructure and heat treatment on thermal conductivity of rheocast and liquid die cast Al-6Si-2Cu-Zn alloy

**M. Payandeh[1]\*** ⓘ **, E. Sjölander[2], A. E. W. Jarfors[1]** ⓘ **and M. Wessén[1]**

Thermal conductivity of a rheocast component made from Stenal Rheo1 (Al-6Si-2Cu-Zn) alloy was investigated in as-cast, T5 and T6 conditions. The thermal conductivity measurement in different locations showed variation of this property throughout the rheocast component. The results of microstructural investigation revealed that the ratio of solute-lean $\alpha_1$-Al particles formed during slurry preparation to fine solute-rich $\alpha_2$-Al particles formed during secondary solidification had significant influence on thermal conductivity. The reduced amount of solutes in the $\alpha_1$-Al particles was determined as the root cause of higher thermal conductivity. A linear relation between the fraction of precipitates and the increase in thermal conductivity was obtained and silicon in solid solution is shown to have a dominant influence. As silicon was precipitated during the heat treatment, thermal conductivity increased. For an optimal combination of thermal and mechanical properties, it is therefore important to use an ageing temperature above the temperature of Si precipitation.

## Introduction

Thermal conductivity is an important material property for applications where heat is generated and needs to be dissipated, for example in electronic devices and engine components. In addition, thermal conductivity is becoming increasingly important as components are packed more densely, systems are miniaturized and heat dissipation becomes a limiting factor. Understanding of thermal conductivity and how this is affected by both solutes and microstructure is getting more critical. In metals, thermal conductivity mainly depends on electron mean free path. Any lattice disturbance, such as phase boundaries, impurities, alloying elements, vacancies or dislocations will scatter electrons and decrease the thermal conductivity.[1,2]

The ability of lattice disturbances to scatter electrons depends on the particular alloying elements and on the amount of these elements present in solid solution, as Guinier–Preston (GP) zones or precipitates. Atoms in solid solution have the greatest influence on thermal conductivity as they form large numbers of scattering centres in the matrix.[3] A decrease in the number of atoms in solid solution, e.g. by precipitation, generally leads to an increase in thermal conductivity as the number of scattering centres decreases.[4] The formation of GP zones, for example, during natural ageing is an exception where thermal conductivity has been reported to decrease despite a decrease in atoms in solid solution.[5,6] Thermal conductivity thus depends not only on alloy composition but also on the microstructure formed during solidification and on its modification during subsequent transformations in solid state, which makes thermal conductivity of a real component very complex property to understand.

During last four decades, new process such as semi-solid metal (SSM) casting integrated with high-pressure die casting (HPDC) process, or SSM-HPDC offers a number of advantages to standard HPDC for manufacturing complex shaped components.[7] Formation of globular primary α-Al phases (hereafter referred to as $\alpha_1$-Al particle) during slurry preparation are the origin of the unique rheological characteristics and critical for castability. Subsequently, during secondary solidification in the die cavity, the remaining liquid melt solidifies and forms fine secondary α-Al phases (hereafter referred to as $\alpha_2$-Al particle).[8,9] Due to the microstructural characteristics in SSM-HPDC casting and limitations on alloy composition which are not commonly encountered in HPDC components,[10] it is important to understand material properties of components produced in the SSM-HPDC process.[11]

The current study focuses on thermal conductivity of a rheocast component made from Stenal Rheo1 (Al-6Si-2Cu-Zn) alloy and the influence of microstructure on thermal conductivity. As a reference to the influence of the SSM-HPDC processing, permanent mould, or die cast material was used. Furthermore, as rheocasting makes the possibility for both T5 and T6 heat treatment process following the casting process, the effect of these heat treatments on thermal transport properties was also investigated.

## Experimental

### Rheocasting

Samples were produced using a 400-ton HPDC machine equipped with an automated RheoMetal™ slurry generator.

[1]Department of Materials and Manufacturing, School of Engineering, Jönköping University, 551 11 Jönköping, Sweden, [2]Scania CV AB, Materials Technology, 15187 Södertälje, Sweden

\*Corresponding author, email mostafa.payandeh@ju.se

The RheoMetal™ included the usage of a so-called enthalpy exchange material (EEM) as an internal cooling agent to generate the slurry.[12] The studied component was an experimental cavity filter demonstrator similar to what is used in telecom base stations. The fixed half die temperature was set to 230–250 °C, while the moving half was set to 280–320 °C. The shot weight was approximately 5 kg and the holding furnace temperature was set to 675 °C. Ladling was done with a standard cast iron ladle to which the EEM was added (5–6% of the shot weight) under stirring (900 rpm) to generate a slurry with a solid fraction of around 40%. The final slurry temperature was at 610 ± 1 °C. The die cavity fill-time was 31 ms with the first stage and the second stage piston speed at 0.23 and 5.2 m/s, respectively. These conditions were similar to standard settings for this type of component under normal HPDC processing.

The composition of the alloy was measured using optical emission spectroscopy (Spectromax™) calibrated with a certified Al–Si–Mg–Cu reference, Table 1. For thermal and microstructural investigation, samples were extracted from the rheocast demonstrator component from three different positions, Figure 1*a*; the wall near-to-gate (position 1), the base plate near-to-gate (position 2) and the base plate near-to-vent (positions 3).

## Liquid die casting

The rheocast material was remelted and cast in a copper mould, Figure 1*b*, to simulate conventional liquid die casting. The mould was disc-shaped with a diameter of 65 mm and a thickness of 10 mm with a feeder. The samples were tested in different conditions: as-cast, T5 heat treated and T6 heat treated.

## T5 heat treatment

Both rheocast and liquid die cast materials were artificially aged at 200, 250, 300 and 350 °C. Ageing curves (hardness vs. ageing time) were produced for samples aged at these temperatures for times between 0 min (only heating) up to 78 h. Ageing curves were evaluated for T5 treatments at 200, 250, 300 and 350 °C to select three conditions of interest for further investigation.

## T6 heat treatment

Solution treatment was conducted at 495 °C. The duration for the solution treatment was adjusted for the differences in coarseness of the microstructures resulting in 9 and 3.5 h for the rheocast and liquid die cast alloys, respectively. The samples were quenched in 50 °C water and subsequently naturally aged for 24 h followed by artificial ageing at 200 °C. Ageing times of 1, 4, 10 and 38 h were used and the ageing curves for 200 °C was analysed for the rheocast material in order to find the peak aged condition. Samples for physical and mechanical properties were then artificially aged to peak aged condition.

## Hardness

Samples for hardness testing were taken from position 1 (the rheocast component). These samples were kept at room temperature for some weeks after heat treatment before hardness measurements were made. The samples were prepared by grinding using 600 mesh or finer SiC paper. Hardness was measured using a Vickers indenter, and a load of 20 kg. The Vickers hardness values calculated based on the values of at least five indentations.

## Microstructure

The microstructure of the rheocast component was investigated. Samples to study micro- and macrosegregation and thermal diffusivity were collected from the same location. The samples were polished and etched using 10% NaOH etchant. The microstructural observations and quantitative measurements such as particles size was made by means of an Olympus Stream™ image analysis system, using contrast-based recognition and a particle size discrimination. Particles size measurements were made on at least six representative images based on area over perimeter measurements. Using the concept of contiguity, $C$ defined as[13]:

**Table 1  Chemical compositions of the Stenal Rheo1 alloys (by mass percentage)**

| Alloy | Si | Fe | Cu | Mn | Mg | Zn | Ti | Cr | Al | $T_L$(°C) |
|---|---|---|---|---|---|---|---|---|---|---|
| SR1 | 5.7 | 0.53 | 2.2 | 0.27 | 0.03 | 0.72 | <0.01 | <0.01 | Balance | 615 |
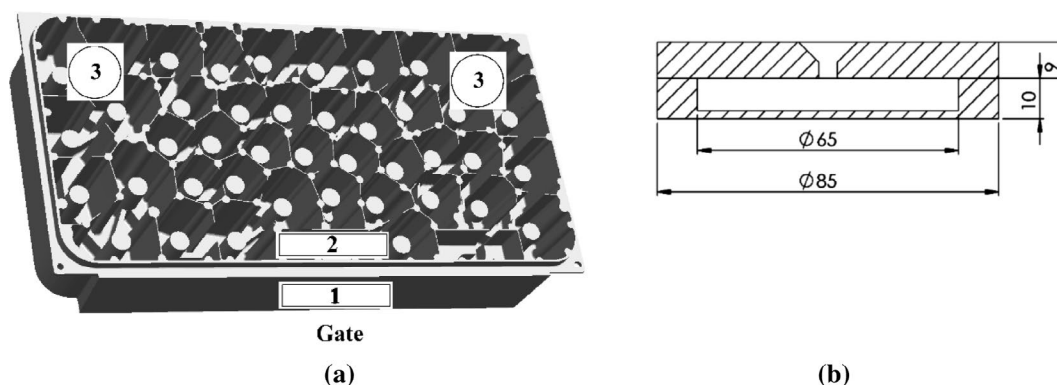


1  *a* Rheocast component. Numbers show the sampling locations, *b* Permanent mould
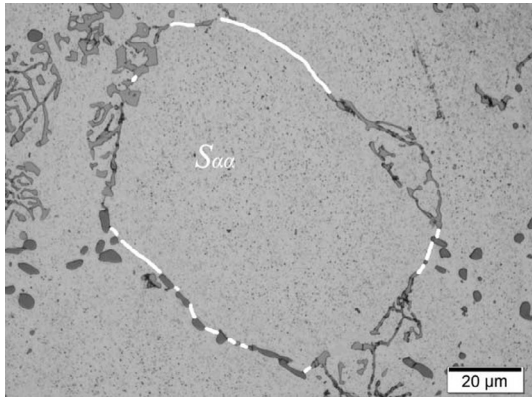
2 The methodology for measuring the $S_{\alpha\alpha}$ for heat-treated sample; the white line indicates the **$S_{\alpha\alpha}$** and the remainder of the particle perimeter is $S_{\alpha\beta}$

$$C = \frac{2S_{\alpha\alpha}}{2S_{\alpha\alpha} + S_{\alpha\beta}} \quad (1)$$

where $S_{\alpha\alpha}$ is the perimeter length of primary Al phase ($\alpha_1$-Al particles for rheocast samples or $\alpha$-Al dendrites for liquid die cast samples) shared with the neighbouring primary $\alpha$-Al phase, while $S_{\alpha\beta}$ is the perimeter of primary $\alpha$-Al phase shared with the other phases such as secondary Al phase ($\alpha_2$-Al phase for rheocast samples) and eutectic phase. The concept of $S_{\alpha\alpha}$ is illustrated in Figure 2 as white lines for a primary $\alpha$-Al phase in a T6 heat-treated rheocast sample. For this study, the mean value of contiguity and standard deviation calculated for 100 $\alpha_1$-Al particles for rheocast samples and $\alpha$-Al dendrites for liquid die cast samples were measured for as-cast and heat treatment condition.

The distribution of Cu and Si inside $\alpha_1$-Al and $\alpha_2$-Al particles in as-rheocast material from position 1, and in $\alpha$-Al dendrites in liquid die cast material were measured using a scanning electron microscope (SEM) equipped with a wavelength dispersive spectrometer (WDS), Figure 3. The concentration of Cu and Si in the matrix of solution heat-treated material was measured in the same way. The acceleration voltage was 20 kV for Cu and 10 kV for Si measurements, using the pure elements as standards. Six dendrites and four $\alpha_1$-Al particles were measured.
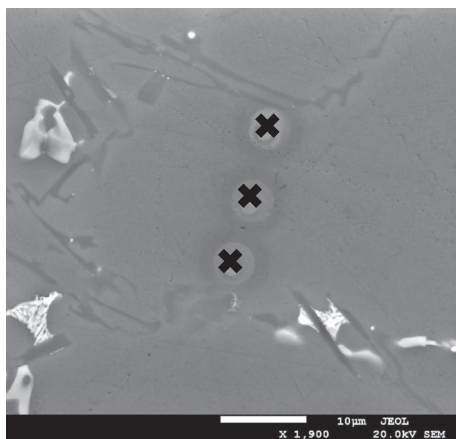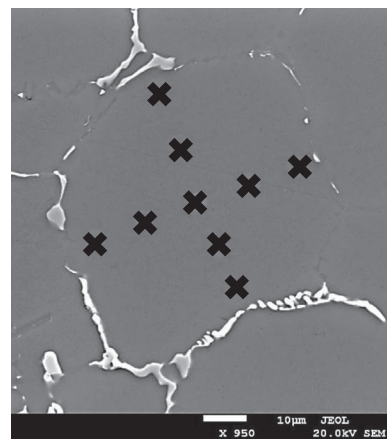
Intermetallic particles were identified using energy dispersive spectrometer (EDS).
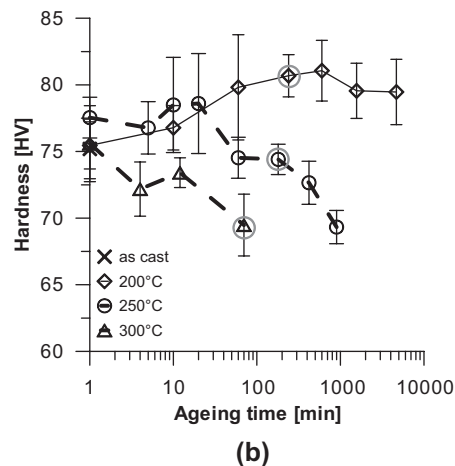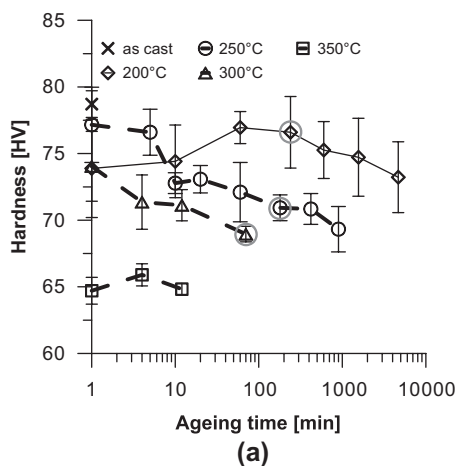
## Physical properties

Thermal conductivity, $\lambda$, was calculated using equation (2). The values for thermal diffusivity $a$, specific heat $c_p$, and density $\rho$, were measured at different temperatures. Thermal diffusivity was measured using a Netzsch LFA 427 laser flash apparatus. Disc-shaped samples 12.5 mm diameter and heights in the range between 3.4 and 3.8 mm were used. These dimensions were selected by means of an optimization process to achieve the most accurate thermal diffusivity. A thin layer of graphite was applied to the samples for optimum laser energy absorption. Thermal diffusivity was measured at 9 temperatures between 30 and 400 °C. Five measurements, with one minute intervals, were made at each temperature.

$$\lambda(T) = a(T) \cdot c_p(T) \cdot \rho(T) \quad (2)$$

Specific heat was measured with a Netzsch DSC 404C differential scanning calorimeter. The samples were heated to 500 °C and cooled slowly (1.5 °C /min) before the measurement. A sample weight of 42 mg and a sapphire standard were used. The heating rate was set to 10 K/min. The specific heat obtained was compared with data from a review by Mills *et al.*[14] of thermophysical properties. Density at room temperature was determined using Archimedes' principle to be $2.70 \pm 0.02$ and $2.74 \pm 0.01$ g/cm$^3$ for the samples from liquid die cast and rheocast materials, respectively. Densities at elevated temperatures were calculated using equation (3). The thermal expansion coefficient $\alpha$, was measured using a Netzsch DIL402C dilatometer. Three samples for each condition were used for thermal diffusivity, calorimetry and dilatometry measurements.

$$\rho(T) = \frac{\rho(T_{RT})}{\left(1 - \alpha\left(T - T_{RT}\right)\right)^3} \quad (3)$$

Phase transformations in the as-cast and T5 conditions were studied using calorimetry for the samples prepared from both rheocast and liquid die cast material. A sample weight of about 20 mg was used. Samples were heated to 500 °C (10 K/min) and then slowly cooled (2 K/min) to room temperature to reach equilibrium condition, after which a second heating cycle was conducted (10 K/min). The calorimetry signal from



(a)



(b)

3 Positions of the WDS points for Cu and Si measurements for the as-cast condition. *a* Liquid die cast and *b* rheocast materials

4   Hardness for T5 treatments for *a* rheocast and *b* die cast material. Conditions marked with grey circles are those used for thermal conductivity measurements

the second heating was then subtracted from the first cycle. The resulting curve peaks are caused by precipitation and dissolution.

## Results

### Determination of optimum heat treatment conditions

#### T5 treatment

Ageing curves were evaluated for T5 treatments at 200, 250, 300 and 350 °C to select three conditions of interest for further investigation. T5 treatment at all temperatures resulted in a decrease in hardness compared to the as-rheocast condition, Figure 4*a*. The ageing curve at 200 °C shows a peak between 60 and 240 min. with hardness close to the as-cast condition. The hardness curves at 250 and 300 °C decreased with time and the hardness at 350 °C reached a low and stable hardness immediately after reaching the ageing temperature.

The ageing response for the die cast material, Figure 4*b*, were similar to that of the rheocast material, but the absolute hardness values were generally higher. Peak hardness was obtained at 200 °C. Three conditions for further study of thermal conductivity were chosen, based on the hardness response: ageing for 240 min. at 200 °C corresponding to peak hardness, for 180 min. at 250 °C to represent an overaged condition and 70 min at 300 °C which is heavily overaged with a low hardness.

#### T6 treatment

Blistering occurred in the thin-walled sections of the rheocast component during solution treatment, hence the T6 treatment was unsuitable for the component under the current processing conditions. The T6 treatment was made for the samples taken from thick-walled sections (4 mm). Solution treatment times were chosen based on the distance between $Al_2Cu$ phases for the two casting processes; $80 \pm 20$ μm for the rheocast material and $50 \pm 10$ μm for die cast material, resulting in solution treatment durations of 9 and 3.5 h for the rheocast and die cast materials, respectively.

The T6 ageing response for ageing at 200 °C for the rheocast material is presented in Figure 5. Peak hardness is obtained between 2 and 10 h. An ageing time of 10 h was decided as it was regarded to be preferable as it was expected
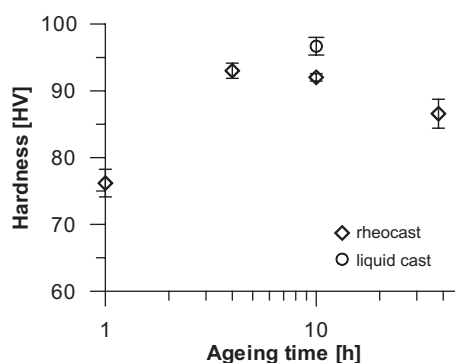


5   Hardness curves after ageing both rheocast and liquid die cast materials at 200 °C for varying times

to give a higher thermal conductivity.[15,16] The liquid die cast material has a higher hardness than the rheocast material after 10 h of ageing.

## Microstructure

### General Features

Figure 6 shows a typical as-rheocast microstructure of the Stenal Rheo1 alloy. The microstructure consists of coarse $\alpha_1$-Al particles, formed during the slurry preparation and fine $\alpha_2$-Al particles formed during solidification of the remaining liquid portions of the slurry in the die cavity. The finer scale of the $\alpha_2$-Al particles was a result of the higher cooling rate during solidification in the die cavity.

Figure 7*a–c* shows the microstructures for the three different locations in the rheocast component; (a) position 1 – wall near-to-gate, (b) position 2 – plate near-to-gate, (c) position 3 – plate near-to-vent. Figure 7*d* illustrates the microstructures of liquid die cast material. The microstructure varies between the different locations in rheocast component. As seen in Figure 7*a* and *c*, the microstructures at position 1 and position 3 were similar. These microstructures contain a larger fraction of fine $\alpha_2$-Al particles solidified in the die cavity. A higher fraction of $\alpha_1$-Al particles was observed in position 2, plate near-to-gate, Figure 7*b*. The inhomogeneity of the microstructure was most likely a result of the separation of the solid and liquid portions of the slurry. The separation was expected to occur during injection of the slurry into the die cavity. As the pressure in the slurry
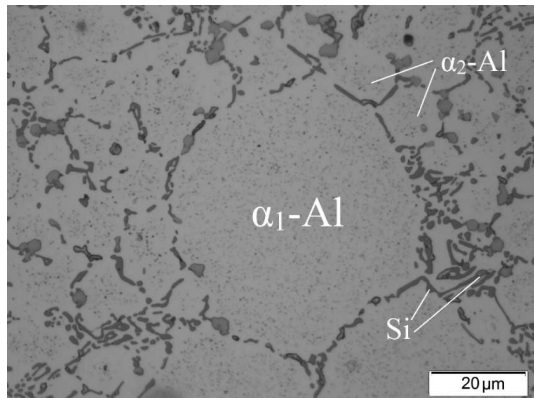
6 Typical microstructure of the as-rheocast material showing coarse $\alpha_1$-Al particles, fine $\alpha_2$-Al particles and Si eutectic

increases during the initial phase of filling process of the die cavity, the liquid phase as a more mobile phase, preferentially forced into the gating system and enters into the die cavity ahead of the solid portion of the slurry. Subsequently, during the later stages of injection the solid $\alpha_1$-Al particles together with some entrapped melt were pushed into the region near-to-gate (Figure 7*b*). On the other hand, the microstructure of the liquid die cast material, Figure 7*d*, showed a dendritic network of $\alpha$-Al and a more uniform microstructure. Figure 7*a* and *c* also shows porosity due to air entrapment and shrinkage porosity at positions 1 and 3. This was most likely a consequence of increased turbulence (due to the lower melt viscosity) after separation of the liquid phase in the gating system, especially as the fill time of the cavity for the current study was similar to traditional HPDC casting.

The microstructure of solution heat-treated materials was investigated. Figure 8 shows an optical micrograph of the rheocast material after solution treatment. It is clear in the

microstructure that fragmentation as well as spheroidization of Si eutectic particles during solution treatment resulted in smaller and rounded Si particles.

### Si and Cu content in the matrix phase

The distribution of Si and Cu in the primary Al phase ($\alpha_1$-Al particles for rheocast material and $\alpha$-Al dendrites for the liquid die cast material) is shown in Figure 9. The Cu content was similar for the rheocast material and the liquid die cast material. In the as-cast condition, the Si concentration in the die cast material showed the expected element distribution due to segregation, while the Si concentration in the rheocast material was more homogenous indicating element homogenization during slurry preparation. The $\alpha_1$-Al particles should therefore have a Si concentration corresponding to the solubility of Si in Al phase at the slurry formation temperature, i.e. 0.89 wt.% Si as calculated using the JMatPro™ software with Al-DATA database.[17,18] The average measured Si concentration was slightly higher, $0.94 \pm 0.07$ wt.% , but the calculated equilibrium concentration is within the measurement error. The $\alpha_2$-Al phases in the rheocast material showed higher concentrations of alloying elements, $1.2 \pm 0.1$ wt.% Si and $0.9 \pm 0.3$ wt.% Cu. This was expected as Si and Cu are enriched in the remaining liquid phase of the slurry due to the formation of $\alpha_1$-Al particles.[19]

The concentration of Si and Cu in the $\alpha_1$-Al particles for solution-treated rheocast and liquid die cast material displays near identical concentrations as $Al_2Cu$ phases dissolved. The measured concentrations of Cu and Si for both rheocast and liquid die cast solution-treated materials was; 2.2–2.3 wt.% Cu and 0.8 wt.% Si. These concentrations are in agreement with the equilibrium concentration calculated for 495 °C using JMATPro™. The phases remaining post solution treatment were rich in Mn, Fe as well as Cr. These phases had a Cu concentration in the range between 3 and 6 wt.% . It can be concluded that successful solution treatments were
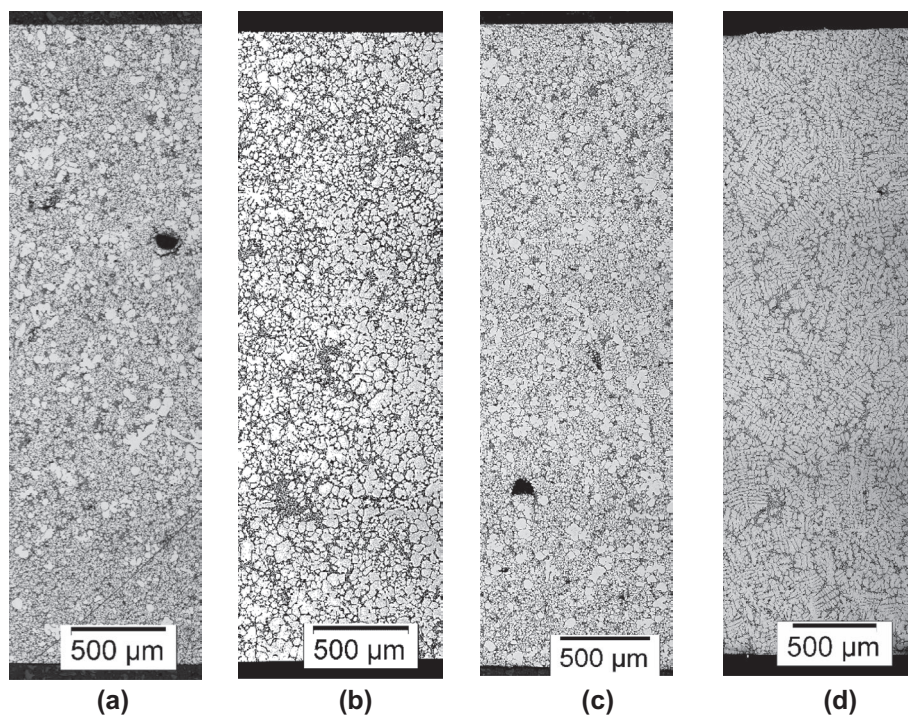


7 Microstructure of as-rheocast component in *a* position 1, *b* position 2 and *c* position 3 and *d* liquid die cast material
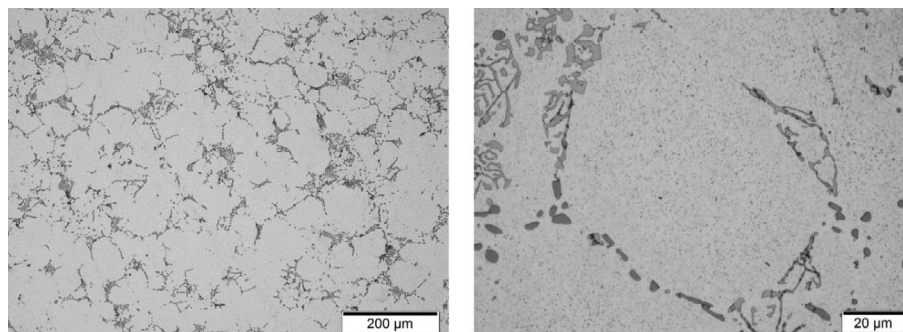
8    Optical micrographs of rheocast component after solution treatment at 495 °C for 9 h
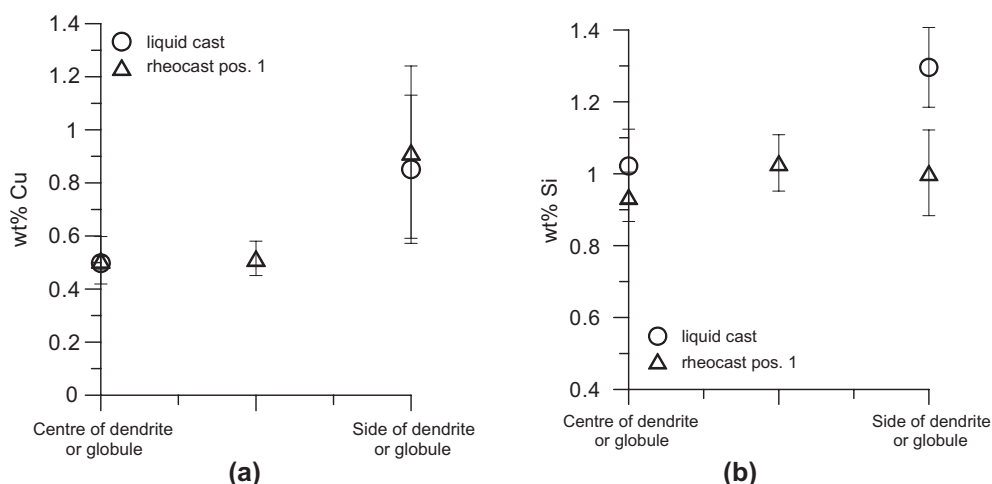


9    Concentrations of *a* Cu and *b* Si in solid solution for the as-cast condition in $\alpha_1$-Al particles for the rheocast materials and in $\alpha$-Al dendrites for the liquid die cast material

**Table 2    Quantification of the microstructure in the as-rheocast and as-cast material in different positions**

| | *fs*(%) rheocast $\alpha_1$-Al particles | | |
| | *fs*(%) die cast $\alpha$-Al dendrites | Contiguity (%) | *fs* × Contiguity |
| --- | --- | --- | --- |
| F pos1 | 27 ± 4 | 3.2 ± 0.6 | 86.4 ± 20.64 |
| F pos2 | 72 ± 6 | 6.4 ± 0.7 | 460.8 ± 63.36 |
| F pos3 | 22 ± 2 | 1.7 ± 0.3 | 37.4 ± 7.42 |
| F liquid | 56 ± 4 | 1.2 ± 0.5 | 67.2 ± 28.4 |

performed, giving high concentrations of Cu in solid solution for both the rheocast and liquid die cast solution-treated materials.

### Microstructural evaluation

Table 2 shows the amount of primary $\alpha$-Al phase (*fs*) and contiguity in the as-rheocast material for the samples from different locations in the rheocast component and for the liquid die cast reference material. In the as-cast condition, the phase with highest conductivity is the primary Al phase ($\alpha_1$-Al particles for rheocast material or $\alpha$-Al dendrites for liquid die cast material). These phases have lower amounts of dissolved elements (confirmed by WDS measurement, Figure 9) than $\alpha$-Al formed during the eutectic reaction. The fraction of $\alpha_1$-Al particles at positions 1 and 3 in as-rheocast material was similar and was approximately one-third of that found at position 2. The contiguity at position 2 was higher as a result of the higher fraction of $\alpha_1$-Al particles. Concomitantly,

positions 1 and 3 showed lower values for *fs* and thereby also a lower contiguity. In the liquid die cast reference material, the fraction of primary $\alpha$-Al dendrite was 56 ± 4%. The lowest contiguity as seen in the liquid die cast alloy is due to the interdendritic eutectic phase.

Similarly, Table 3 shows these microstructural characteristics for T5 and T6 conditions for the rheocast and the liquid die cast materials. The *fs* values for the T5 and T6 conditions now includes all the $\alpha$-Al phase as these are chemically identical due to the homogenization of dissolved elements in the $\alpha$-Al phase. This equilibration will cause a similar thermal conductivity across the $\alpha$-Al phase which was not the case for the as-cast condition. Compared to T5-treated material, the microstructural characterization of T6-treated material showed a significant increased contiguity. This was caused by a change in morphology of Si-particle during the T6 treatment at 495 °C where the Si-particles were fragmented and spheroidized.

**Table 3    Quantification of the microstructure in the heat-treated material**

|  | *fs*(%) α-Al phases | Contiguity (%) | *fs* × Contiguity |
|---|---|---|---|
| T5- pos1 | 88 ± 4 | 3.3 ± 0.6 | 290.4 ± 54.42 |
| T5- liquid | 86 ± 4 | 1.5 ± 0.5 | 129 ± 43.41 |
| T6- pos1 | 90 ± 3 | 66 ± 6 | 5940 ± 575.15 |
| T6- liquid | 83 ± 2 | 48 ± 5 | 3984 ± 425.95 |
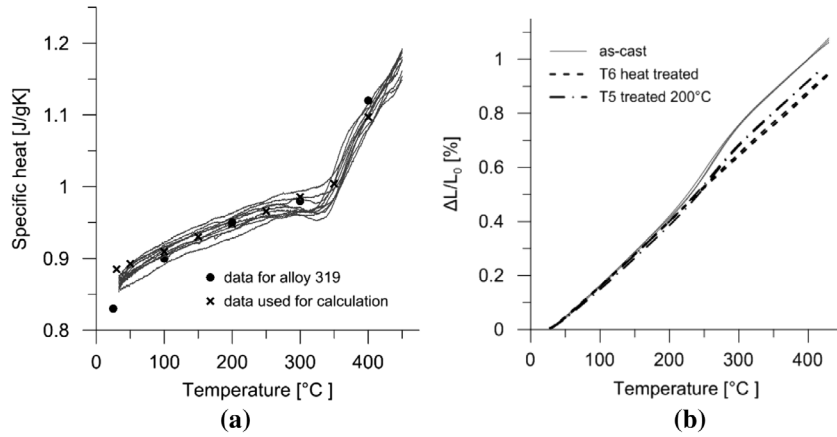


10  *a* Specific heat for alloy 319 and for Stenal Rheo1, *b*, thermal expansion for the liquid die cast and the rheocast materials showing no difference between the two methods of casting

**Table 4    Thermal expansion coefficients [$10^{-6/K}$] for as-cast and heat-treated samples. Average values and standard deviations**

| Temperature | as-cast | | T5 200 °C | | T5 $T \geq 250$ °C and T6 | |
|---|---|---|---|---|---|---|
| interval [°C] | Average | std | average | std | Average | std |
| 30–200 | 24.6 | 0.2 | 23.3 | 0.5 | 23.4 | 0.3 |
| 200–315 | 33.3 | 0.5 | 28.4 | 0.6 | 24.5 | 0.3 |
| 315–430 | 23.8 | 1.0 | 23.5 | 0.6 | 23.2 | 0.2 |

## Physical properties

### Specific heat and thermal expansion

The apparent (average) specific heat was measured at 100, 150, 200, 250 and 400 °C and the results are shown in Figure 10 (a). These curves include the energy absorbed or released due to dissolution and precipitation events during heating. This energy should not be included in the specific heat and for that reason a curve was fitted to the data for the temperature region 100–250 °C. The specific heat at 30, 50, 300 and 350 °C was then extrapolated from the fitted curve. The data used for the calculation of thermal conductivity is indicated in Figure 10*a* with crosses. The results from this investigation are in accordance with data presented in a review[14] for an A319 alloy similar to Stenal Rheo1. The data for the specific heat were used for the calculation of thermal conductivity for the T5- and T6-treated samples as well.

Thermal expansion is presented in Figure 10*b* and thermal expansion coefficient is collated in Table 4, respectively. There was no difference in thermal expansion between the liquid die cast and the rheocast material. The materials in as-cast condition showed an increase in thermal expansion starting around 210–220 °C. In the T5 treated at 200 °C, the thermal expansion curve was situated between that for as-cast and T6-treated samples, see Figure 10*b*. An average thermal expansion for T5 treated above 250 °C and for T6-treated materials was used in the calculation of thermal conductivity, Table 4.
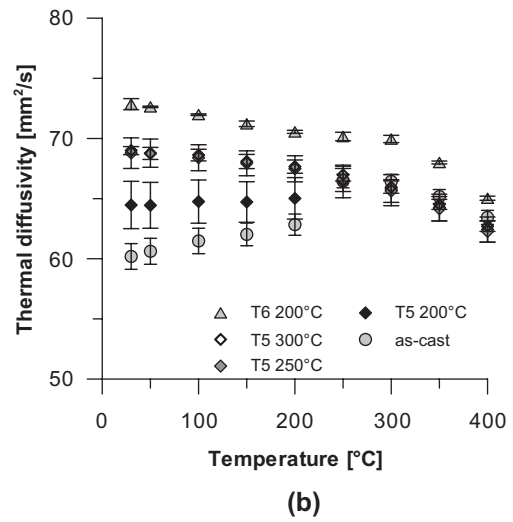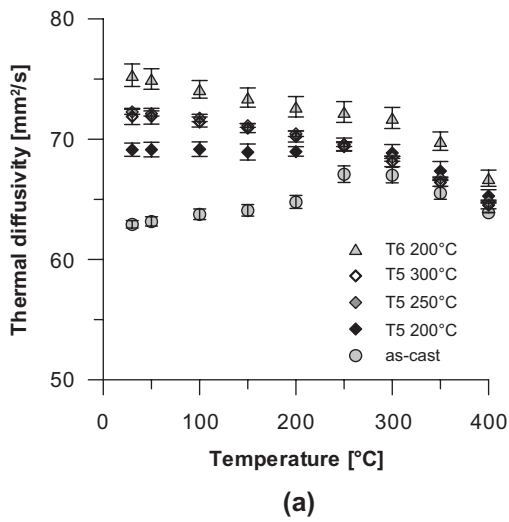
### Thermal diffusivity and conductivity

Thermal diffusivity was measured during heating from 30 to 400 °C, Figure 11*a* and thermal conductivity was calculated using thermal diffusivity, specific heat and thermal expansion, Figure 11*b,* respectively. The rheocast materials showed a higher thermal diffusivity than the liquid die cast material. In the rheocast materials, the location in the component and the associated microstructure influenced the thermal diffusivity. The thermal diffusivity at position 2 was higher than at positions 1 and 3 and position 1 was slightly higher than position 3. The liquid die cast material consistently showed the lowest thermal diffusivity. In all the cases, the differences decreased with increasing temperature, but the relative order remained the same.
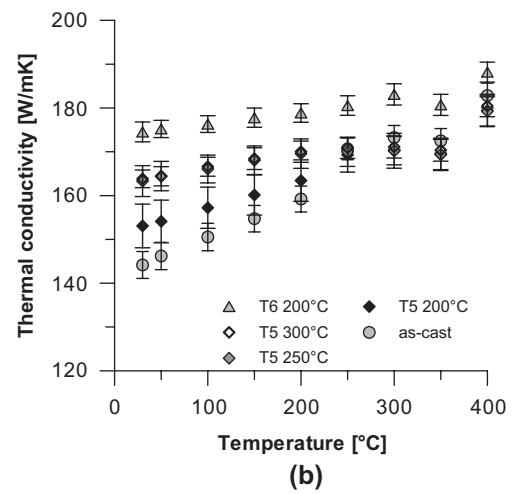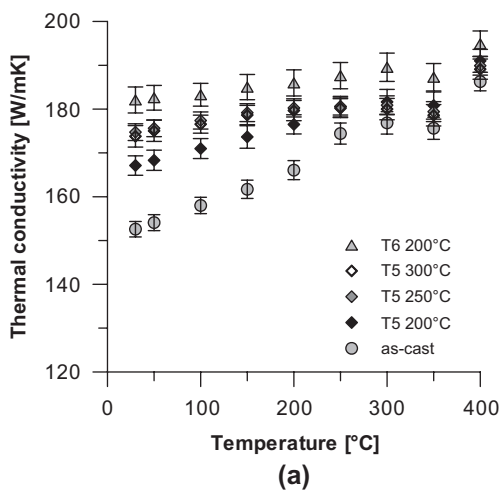
Thermal diffusivity and thermal conductivity of heat-treated rheocast and the liquid die cast material are shown in Figs. 12 and 13, respectively. All treatments resulted in an increase in thermal diffusivity compared to the as-cast condition for both the rheocast material and the liquid die cast material. The thermal conductivity after the T5 treatment at 250 and at 300 °C was about the same, while a T5 treatment at 200 °C resulted in a lower thermal conductivity. A T6 treatment resulted in further increasing in thermal diffusivity and conductivity compared to the T5 treatments. Furthermore, the difference in diffusivity between the rheocast and the liquid die cast material for the as-cast condition, Figure 11*a*, remained after a T6 heat treatment suggesting that there were
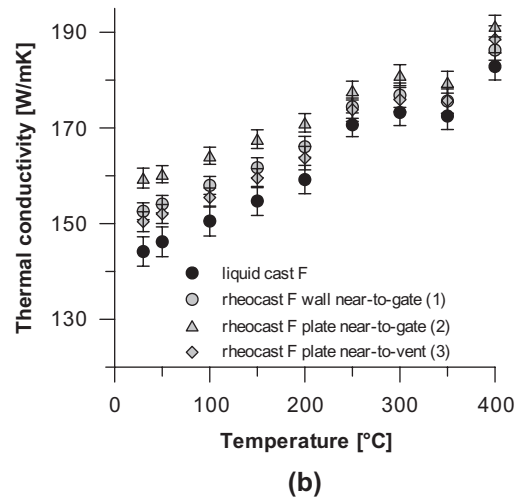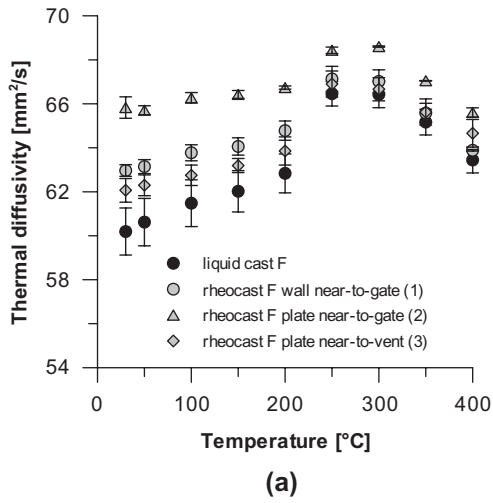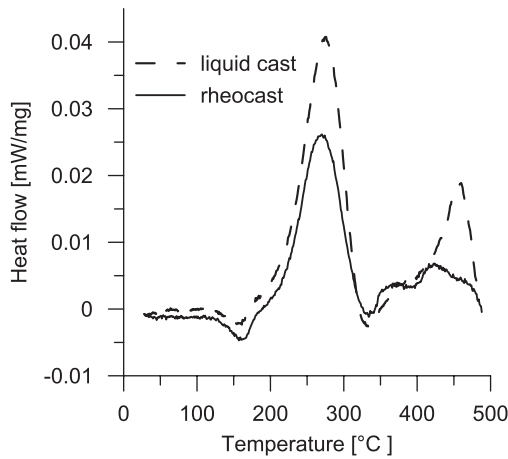
**11** *a* Thermal diffusivity and *b* conductivity of the rheocast and the liquid die cast materials in the as-cast condition
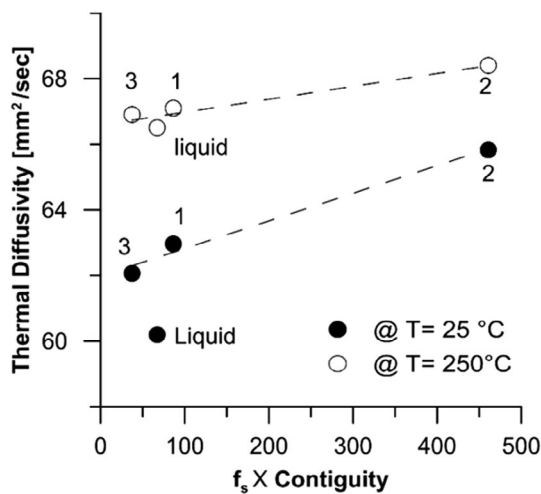


**12** Thermal diffusivity of T5- and T6-treated *a* rheocast and *b* liquid die cast material



**13** Thermal conductivity of T5- and T6-treated a rheocast and b die cast materials

14 **The precipitation sequence for the liquid die cast and rheocast material in the as-cast condition**



15 **Effect of primary particle characteristics on thermal conductivity at room temperature and at 250 °C in the rheocast and liquid material die as cast conditions.** (*fs* is fraction of α₁-Al particles. Numbers indicate the position of sample in the rheocast component)

some fundamental differences caused by the nature of the microstructure and not by the solutes.

## Precipitation processes

The precipitation sequence of the as-cast liquid and rheocast material is presented in Figure 14. Both graphs show a clear peak around 225–325 °C, corresponding primarily to the precipitation of dissolve elements from solid solution. However, the larger peak area of the liquid die cast material clearly indicates that higher amount of precipitates were formed. This result explicitly shows a good agreement with the result from WDS measurement, (see Figure 9*b*).

## Discussion

Both thermal conductivity and electrical conductivity are influenced by electron transport in metal alloys.[20] As well, the electron mean free path is strongly decreased by lattice perturbation such as impurities, solutes, vacancies and dislocations. The ability of electrons to percolate an inhomogeneous
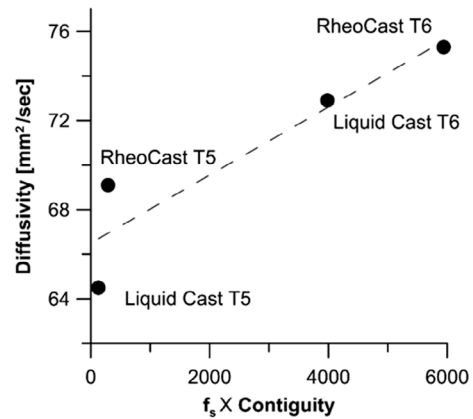


16 **Microstructural effect on thermal conductivity of heat-treated condition (fs is fraction alpha phase)**

microstructure depends on the characteristics of the conducting phases such as volume fraction, the conductivity of these phases as well as the nature of contact between these phases.
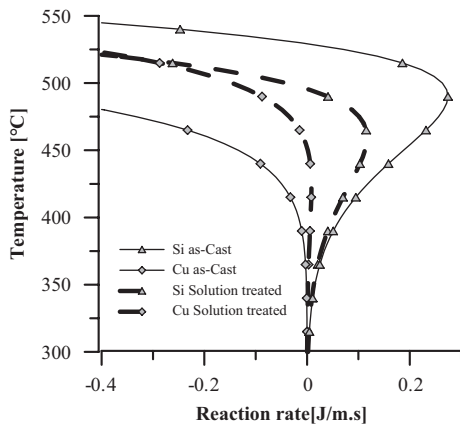
## The as-cast condition

Thermal diffusivity and microstructure varied at different locations in the as-rheocast component. The thermal diffusivity results from position 2 showed a higher diffusivity than position 1 and 3 at all temperatures, Figure 11*a*. At room temperature, Figure 15, the thermal diffusivity at the three locations is related to the fraction as well as contiguity of α₁-Al particles (from Table 2). In the rheocast material, thermal diffusivity increased from 62 (position 3) to 66 mm²/s (position 2). Similarly, the fraction of the conducting α₁-Al particles and their contiguity increased. It was also observed that the slope of the trend line decreased at higher temperature, while the difference in thermal diffusivity between the positions decreased as well. This decrease was likely a result of precipitation that took place between 200 and 350 °C shown through DSC.
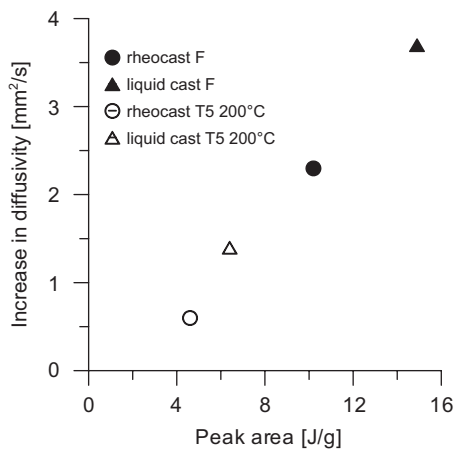
As the temperature was increased from 25 to 250 °C, the difference between thermal diffusivity of the rheocast and the liquid die cast material decreased significantly as the change in conductivity of the die cast material was significantly higher (3.7 mm²/s) compared to the rheocast material (2.3 mm²/s). This can be explained by the higher amount of Si in solid solution in the as-die cast material, Figure 9*b*. This suggested that a larger amount of precipitation occurred when heating to 250 °C, shown as greater increase in diffusivity.

## T5-treated condition

Higher thermal diffusivity was observed for samples subjected to a T5 treated at 250 and 300 °C compared to those treated at 200 °C. This was observed for both the rheocast and the liquid die cast material. In Figure 15, the increase in thermal diffusivity is shown closely related to the amount of precipitation taking place in the material suggested to be precipitating from the supersaturated matrix. By raising the temperature to 250 °C during the diffusivity measurement, dissolved Si and Cu precipitated and the thermal diffusivity of the T5-200 °C-treated samples increases and reaches a value similar to that of T5-250 °C and T5-300 °C-treated samples. For the liquid die cast alloy, the diffusivity for all T5-treated samples as

**17** The precipitation of Si and Al$_2$Cu as-cast condition (solid line) and solution treatment (dash line)



**18** Increase in diffusivity when the temperature was increased from 200 to 250 °C vs. peak area for Si precipitation

well as the as-cast samples converge at 250 °C. For the rheocast material, the thermal diffusivity in the as-rheocast materials still had a lower value at 250 °C compared to the T5-treated materials. This was expected as a result of the larger variation in microstructure of the rheocast material compared to the liquid die cast material.

## T6-treated condition

T6 heat-treated samples shows higher thermal diffusivity, Figure 12 as well as higher thermal conductivity, Figure 13, compared to T5 treated and as cast conditions for both liquid die cast and rheocast material. The thermal diffusivity in T6-200 °C and T5-200 °C-treated samples are compared in Figure 16.

For the rheocast material, the difference in thermal diffusivity at room temperature between the T5 and T6 conditions is 6.2 mm$^2$/s, which corresponds to a difference of 15 W/mK in thermal conductivity. This difference was primarily caused by differences in the amount of dissolved Si and Cu in solid solution. Dilatometry and calorimetry measurements indicated that presence of these elements in solid solution after a T5-200 °C treatment compared to other treatments. This was assumed to be due to shorter ageing time for the T5 heat treatment (4 h) compared to the T6 treatment (10 h). The effect was not as strong in the T5 sample as the solution treatment

was omitted and contiguity did not change significantly. This effect was removed after heating to 250 °C and the difference in thermal diffusivity decreased to 2.7 mm$^2$/s and remained constant until it decreased to 1.5 mm$^2$/s at 400 °C.

The T6 heat treatment was observed to lead to rounder Si particle, Figure 8. This morphological change increased contiguity.[21] In contrast to T6-200 °C samples, where the main difference between the liquid die cast and the rheocast material was likely due to differences in microstructure, in the T5-200 °C condition this difference cannot solely be due to differences in the microstructure and the effect of solutes and precipitates must be considered. The effects of relevant microstructural differences are briefly discussed in relation to their effect on thermal conductivity:

- The concentration of Mn in solid solution is expected to decrease during solution treatment due to precipitation of Mn containing dispersoids, which will result in an increase in thermal conductivity.[22]
- The concentration of Cu in solid solution increases from 0.5 wt.% to 2.2–2.3 wt.% during solution treatment, which is expected to result in a higher fraction of $\theta''$ precipitates formed during ageing. The influence of these Cu-containing precipitates on diffusivity depends on their size.[5,6] When they become large, they will have a small influence similar to that of Al$_2$Cu particles.
- During solution treatment, the concentration of Si dissolved in the matrix was reduced from 1.1 wt.% to 0.8 wt.%. A lower volume fraction of Si precipitates is thereby expected to form during ageing of the solution-treated material, which is expected to give a higher diffusivity.

### *Silicon precipitation –thermal diffusivity relationship*
The precipitation sequence of the as-cast liquid and rheocast material, Figure 14, indicated a clear peak around 225–325 °C. However, the larger peak area of the die cast clearly indicates that higher amount of precipitates were formed in the die cast sample. Precipitation of both Si and Cu are possible in the alloy[23] and mobility and driving force will determine which alloying element will be dominant driven by temperature and state of the aluminium matrix from a solid solution point of view. The rate of reaction, $v$, can be estimated by the mobility (in this case diffusion rate of element in aluminium matrix), $D$, and driving force, $\Delta G$ as[24]

$$v = D\left(\frac{\Delta}{G}V_m\right) = \frac{DRT}{V_m}\ln\left(\frac{X_i^{\text{matrix}}}{X_i^{\text{eq}}}\right) \qquad (4)$$

where $V_m$ as molar volume, $R$ as general gas constant, $T$ as absolute temperature, $X_i^{\text{matrix}}$ as the actual concentration of solutes in the matrix and $X_i^{\text{eq}}$ as the equilibrium concentration of solutes in the matrix according to the phase diagram. In Figure 17, this is shown for the precipitation of Si and Al$_2$Cu as-cast condition (solid line) and solution treatment (dash line) for the liquid die cast and rheocast materials. The results clearly show that in the as-cast condition Al$_2$Cu is not a stable precipitate above 300 °C. After solution treatment, copper-bearing phases in the eutectic regions dissolve and increase the copper content in solid solution. Comparing to the rate for the precipitation, the precipitation of Al$_2$Cu is significantly slower in both the as-cast condition as well as in the solution-treated condition. Given that both the rate and the total amount of Si are greater, it is possible to conclude that Si is the dominating phase precipitating and the main contributor for the generation of heat from precipitation detected in differential scanning calorimetry.
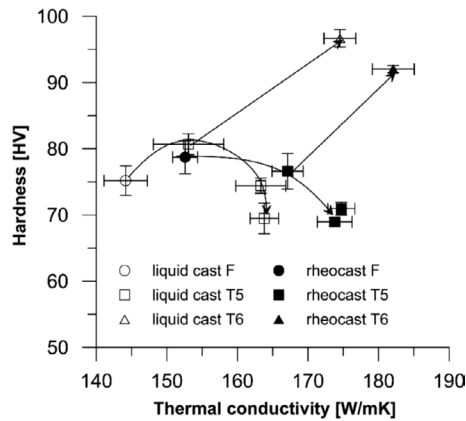
19 Relation between hardness and conductivity, showing for rheocast and liquid die cast materials

Moreover, plotting the amount of released heat during heating for precipitation sequence analysis for the die cast and rheocast material was used to plot the increase in diffusivity when the temperature increased from 200 to 250 °C vs. the peak area related to Si precipitation. The results, see Figure 18, clearly revealed a linear relationship between these parameters. The results indicated that the absence of increase in thermal diffusivity in the temperature range of 250°C and 300°C for the T5 treated samples was related to that all Si was completely precipitated before the LFA measurement. It was proved by the fact that precipitation peak in the calorimetry measurements was not detected in these samples as well. Similar results were also found by Lasagni *et al.* [25]

## Strength – Conductivity relation

Figure 19 shows the relation between hardness and thermal conductivity. An increase in thermal conductivity without a decrease in strength was observed for the T5 treatment at 200 °C. Further increase in the conductivity was obtained by overageing, but with reduced hardness. The T6 treatment provided superior strength and thermal conductivity. Correspondingly, the relation between hardness and thermal conductivity revealed complex behaviour. The reason for the complex behaviour has been attributed to atoms in solid solution, GP zones and precipitates, having different impact on electron mean free path as well as on precipitation hardening.[26]

## Conclusions

The thermophysical properties of the alloy Stenal Rheo1were measured in as-rheocast and heat-treated condition including both T5 and T6 conditions. A reference liquid die cast Stenal Rheo1 was used. In the as-rheocast conditions, thermal conductivity of 153 W/mK at room temperature was achieved. For the same material, in an overaged T5 condition at 250 or 300 °C, a thermal conductivity of 174 W/mK was obtained. In a peak aged T6 condition following ageing at 200 °C, a thermal conductivity of 182 W/mK was achieved. The liquid die cast material displayed lower thermal diffusivity and conductivity for all conditions compared to the rheocast material.

The microstructure of rheocast Stenal Rheo1 consisted of coarse and solute-lean globular $\alpha_1$-Al particles and fine solute-rich $\alpha_2$-Al particles, whereas the liquid die cast sample consisted only of dendritic α-Al. In addition to the fact that the liquid die cast material was dendritic and the rheocast material was globular, there was also macroscale microstructural inhomogeneity in the rheocast material but not in the liquid die cast material. This macroscale inhomogeneity had significant influence on thermal conductivity where in the as-rheocast condition thermal conductivity varied from 150 W/mK in areas with low fraction of $\alpha_1$-Al particles to 160 W/mK in regions with high fractions of $\alpha_1$-Al particles. This difference could be explained by the product of fraction $\alpha_1$-Al particles and its contiguity.

The dominant factor for thermal conductivity was however the influence of Si solutes on thermal diffusivity. Thermal conductivity was significantly increased as Si was precipitated during heat treatment at 200–250 °C. The increase in thermal conductivity displayed a linear relation to the amount of heat evolved during precipitation.

The liquid die cast reference material had higher amounts of solutes in the matrix phase in the as-cast condition, which results in a lower thermal diffusivity and a higher hardness and strength compared to rheocast samples. The difference in thermal diffusivity between the liquid and rheocast alloy was reduced when temperature was raised above 250 °C due to Si precipitation.

Both rheocast and liquid die cast material displayed similar behaviour as each other for the thermal conductivity strength relation. However, the rheocast material had a better conductivity compare to liquid cast material in all conditions but slightly lower in strength with a continued increase in thermal conductivity as a result of overageing condition in the T5 condition and a superior combination of strength and thermal conductivity in the peak aged T6 condition.

## Acknowledgements

## Funding

## ORCID

*M. Payandeh* http://orcid.org/0000-0001-6755-2123
*A. E. W. Jarfors* http://orcid.org/0000-0002-0101-0062

## References

1. H. Fredriksson and U. Åkerlind: 'Physics of functional materials'; 2008, Chichester, West Sussex , England, John Wiley & Sons.
2. Y. S. Touloukian and D. P. DeWitt: 'Thermophysical properties of matter-the TPRC data series', Vol. 7, 'Thermal Radiative Properties-Metallic Elements and Alloys'; 1970, Purdue Univ., Lafayette, IN (United States), Thermophysical and Electrical Properties Information Center.
3. T. M. Tritt: 'Thermal conductivity; theory, properties and applications'; 2004, New York, US, Kluwer Academic/Plenum Publishers.
4. J. E. Hatch:'Aluminum, properties and physical metallurgy'; 1984, ASM International, Materials Park , OH.

5. K. Osamura, N. Otsuka and Y. Murakami: 'Resistivity maximum during Guinier-Preston zone formation in an Al-4 wt% Cu alloy', *Philos. Mag. B*, 1982, **45** (6),583–599.

6. S. Esmaeili, D. Vaumousse, M. W. Zandbergen, W. J. Poole, A. Cerezo and D. J. Lloyd: 'A study on the early-stage decomposition in the Al-Mg-Si-Cu alloy AA6111 by electrical resistivity and three-dimensional atom probe' *Philos. Mag.*, 2007, **87**, 3797–3816.

7. D. H. Kirkwood, M. Suéry, P. Kapranos, H. V. Atkinson, and K. P. Young: 'Semi-solid processing of alloys'; 2009, Berlin, Springer.

8. M. Hitchcock, Y. Wang and Z. Fan: 'Secondary solidification behaviour of the Al–Si–Mg alloy prepared by the rheo-diecasting process', *Acta Mater.*, 2007, **55**, 1589–1598.

9. M. Payandeh, A. Jarfors and M. Wessén: 'Influence of Microstructural Inhomogeneity on Fracture Behaviour inSSM-HPDC Al-Si-Cu-Fe Component with Low Si Content', *Solid State Phenom.*, 2015, **217–218**, 67–74.

10. J. G. Kaufman and E. L. Rooy: 'Aluminum alloy castings: Properties, processes, and applications'; 2004, Materials Park - ASM International.

11. G. Govender and L. Ivanchev: 'Opportunities and Challenges for Use of SSM Forming in the Aerospace Industry', *Solid State Phenom.*, 2006, **116**, 92–95.

12. M. Wessén and H. Cao: 'The RSF technology; 'A possible breakthrough for semi-solid casting processes', *Proc. 3rd Int Conf of High Tech Die Casting* AIM, Vicenza, Italy September 21–22, 2006.

13. J. Gurland: 'An estimate of contact and continuity of dispersions in opaque samples', *AIME Met. Soc. Trans.*, 1966, **236**, 642–646.

14. K. C. Mills: 'Recommended values of thermophysical properties for selected commercial alloys'; 2002, Abington Hall, , Abington, Cambridge,. Woodhead Publishing Limited.

15. E. Cerri, E. Evangelista, S. Spigarelli, P. Cavaliere and F. DeRiccardis: 'Effects of thermal treatments on microstructure and mechanical properties in a thixocast 319 aluminum alloy', *Mater. Sci. Eng., A*, 2000, **284**, 254–260.

16. M. A. Salazar-Guapuriche, Y. Y. Zhao, A. Pitman and A. Greene: 'Correlation of strength with hardness and electrical conductivity for aluminium Alloy 7010', *Mater. Sci. Forum*, 2006, **519–521**, 853–858.

17. N. Saunders: 'The application of calculated phase equilibria to multi-component aluminum alloys', *Keikinzoku/Journal of Japan Institute of Light Metals*, 2001, **51**, 141–150.

18. Z. Guo and W. Sha: 'Quantification of precipitate fraction in Al–Si–Cu alloys', *Mater. Sci. Eng., A*, 2005, **392**, 449–452.

19. S. Ji, A. Das and Z. Fan: 'Solidification behavior of the remnant liquid in the sheared semisolid slurry of Sn–15 wt.% Pb alloy', *Scr. Mater.*, 2002, **46**, 205–210.

20. R. M. German: 'Powder metallurgy science'; Metal Powder Industries Federation, 105 College Rd. E, Princeton, N. J. 08540, U. S. A, 1984. 279 (1984).

21. M. H. Mulazimoglu, R. A. L. Drew and J. E. Gruzleski. 'The electrical conductivity of cast Al-Si alloys in the range 2 to 12.6 wt pct silicon', *Metall. Trans. A*, 1989, **20**, 383–389.

22. L. Lodgaard and N. Ryum. 'Precipitation of dispersoids containing Mn and/or Cr in Al-Mg-Si alloys', *Mater. Sci. Eng., A*, 2000, **283**, 144–152.

23. Y. Birol: 'Response to artificial ageing of dendritic and globular Al-7Si-Mg alloys', *J. Alloys Compd.*, 2009, **484**, 164–167.

24. M. Hillert: 'Diffusion and interface control of reactions in alloys', *Metall. Trans. A*, 1975, **6**, 5–19.

25. F. Lasagni, A. Falahati, H. Mohammadian-Semnani and H. Degischer: 'Precipitation kinetics of Si in aluminium alloys', *Materials Science and Engineering: A*, 2008, 480(1–2), 383–391.

26. M. Natan and R. A. Chihoski: 'Relationship between microstructure, hardness and electrical conductivity of 2219 aluminium', *J. Mat. Sci.*, 1983, **18**, 3288–3298.